PCCP

Accepted Manuscript

ROYAL SOCIETY OF CHEMISTRY

www.rsc.org/pccp

Dissociative dynamics of O_2 on Ag(110)

Ivor Lončarić,[1,*] M. Alducin,[1,2,†] and J.I. Juaristi[3,1,2,‡]

[1] *Centro de Física de Materiales CFM/MPC (CSIC-UPV/EHU), Paseo Manuel de Lardizabal 5, 20018 Donostia-San Sebastián, Spain*

[2] *Donostia International Physics Center DIPC, P. Manuel de Lardizabal 4, 20018 San Sebastián, Spain*

[3] *Departamento de Física de Materiales, Facultad de Químicas, Universidad del País Vasco (UPV/EHU), Apartado 1072, 20080 San Sebastián, Spain*

Abstract

We study the dissociative dynamics of O_2 on Ag(110) by performing classical and quasiclassical trajectory calculations on an adiabatic six-dimensional potential energy surface (PES). The PES is constructed from the interpolation of a large set of energies that are calculated with spin-polarized density functional theory. The minimum energy barrier to dissociation amounts to 0.36 eV. This value, which is considerably lower than the barriers of about 1.1 eV found in the Ag(100) and Ag(111) surfaces, is in line with the measured much higher reactivity of the (110) surface. Our classical dynamics calculations show that at normal incidence conditions no significant dissociation occurs below an initial energy of 0.9 eV (0.6 eV in the quasiclassical calculations). This result is an indication of a very reduced configurational space leading to dissociation and also explains why direct dissociation has not experimentally been observed at low incidence energies. Our calculations also show that for off-normal incidence, most of the dissociation takes place close to the long-bridge site, a region of the configurational space where the energy barriers to dissociation are higher than 0.7 eV, resulting in still lower dissociation probabilities.

PACS numbers: 34.35.+a,79.20.Ap,79.20.Rf

* ivor.loncaric@gmail.com

† wapalocm@ehu.es

‡ josebainaki.juaristi@ehu.es

I. INTRODUCTION

The importance of silver as a catalyst in the epoxidation of ethylene has led to extensive studies on the nature of the interaction of oxygen with silver surfaces. Apart from the technological applications, dynamics of this interaction is interesting from a fundamental point of view as a model gas-metal system with several adsorption states and dissociation processes. Dynamics of oxygen on flat silver surfaces is particularly rich as experiments have identified three distinct adsorption states: a physisorbed state at surface temperatures $T < 40$ K, a molecularly chemisorbed state at $T = 40-150$ K and a dissociative state at $T > 150$ K [1–3]. Molecular beam experiments have showed that the close-packed Ag(111) surface is inert towards oxygen uptake showing extremely low ($\approx 10^{-6}-10^{-5}$) initial dissociative and molecular sticking coefficients [4, 5] for incident kinetic energies below 0.8 eV. In contrast, the molecular sticking coefficients measured at $T \approx 100$ K on Ag(100) [6] and Ag(110) [7] exceed values of 0.5 at the highest incident energies. At higher temperatures ($T \approx 300$ K) the initial sticking probabilities are substantially reduced (in the range of $10^{-2} - 10^{-3}$) on the Ag(100) surface, showing that desorption at this temperature is much more probable than dissociation [6, 8]. The Ag(110), the surface studied in this paper, is the most reactive flat silver surface for O_2 dissociation. In this surface it has been shown that the dissociative sticking coefficient at $T = 300$ K and the molecular sticking coefficient at $T = 100$ K are of the same order of magnitude [7, 9, 10].

Experimental results obtained using molecular beam techniques indicate that the molecular adsorption of O_2 on Ag(110) is an activated process. This has been concluded from the observation that a threshold of about 0.2 eV in translational energy is required for adsorption to occur at normal incidence [7, 9, 10]. The absence of adsorption below this threshold energy has also led to exclude any influence of the physisorption state [7]. Regarding molecular chemisorption, various experimental techniques have shown that O_2 adsorbs parallel to the surface with the molecular axis along the <001> or the <1$\bar{1}$0> direction [11–15]. From the measured temperature dependence of the initial adsorption coefficient it has also been deduced that dissociative adsorption at low incident energies is not direct and that it requires previous adsorption of the molecular species in its chemisorbed state [7, 9, 10]. At higher energies, direct dissociation could not be discarded but appeared to be masked by the more probable indirect dissociation [10].

Density functional theory (DFT) calculations of Gravil *et al.* [16–18] found that the chemisorption position corresponds to the molecule with its center of mass located in a hollow site, parallel to the surface and with equal adsorption energies for both <001> and <1$\bar{1}$0> orientations of the molecular axis. A possible physisorbed state, with an unexpectedly large adsorption energy, was also found corresponding to the molecule with its center of mass in the long-bridge site, parallel to the surface and with the molecular axis oriented along the <001> direction. Contrary to the conclusion of molecular beam experiments that adsorption is activated [7, 9, 10], these calculations did not find entrance barriers to the chemisorption state. Further characterization of the chemisorption state at the DFT level is given in Refs. [19–21]. More recently Roy *et al.* [22] used DFT calculations to simulate STM induced dissociation experiments of Hahn and Ho [14, 15]. In addition to the long-bridge adsorption site, another adsorption position was found at the short-bridge site with the molecule parallel to the surface oriented along the <1$\bar{1}$0> direction with even larger adsorption energy. The energy barriers to dissociation from chemisorption sites were calculated, and found to be similar for both chemisorption orientations.

Aforementioned DFT calculations were focused on specific configurations of the molecule on the surface and give valuable information about adsorption positions and energy barriers to dissociation. Still, full understanding of the complex interaction of the oxygen molecule with the Ag(110) surface at DFT level can only be achieved by performing trajectory calculations. Because of the high computational demand of ab initio molecular dynamics, only small number of trajectories can be calculated, resulting in poor statistics. Dynamics of this system has been previously studied using a model LEPS (London-Eyring-Polanyi-Sato) potential by Pazzi *et al.* [23, 24]. This approach enables to evaluate large numbers of trajectories but introduces empiricism in the potential. On the other hand, if the surface is kept frozen a full (six) dimensional high quality potential energy surface (PES) can be constructed by interpolating a grid of DFT energies. Thousands of trajectories can then be evaluated on this PES providing reliable statistics. This methodology has been already used to study dynamics of oxygen on the Ag(100) [25] and the Ag(111) [26, 27] surfaces, but a similar study on the more reactive Ag(110) is missing. The objective of this paper is to fill this gap. With this aim we construct such DFT-PES, examine its features and perform classical and quasiclassical trajectory calculations. The construction of the potential energy surface is described in Section II. The PES is examined in Section III, where we discuss adsorption

energetics and positions, as well as paths and energy barriers to dissociation. In Section IV we present and discuss results of the trajectory calculations. The main conclusions of the paper are summarized in Section V.

II. CALCULATION OF THE ADIABATIC POTENTIAL ENERGY SURFACE

In the adiabatic picture, the interaction of the O_2 molecule and the frozen Ag(110) surface is fully described by a six-dimensional (6D) potential energy surface (PES) that only depends on the position of the two O atoms over the surface. Here, we construct the continuous 6D PES by interpolating with the *corrugation reducing procedure* (CRP) [28] a set of 25 376 energies that are calculated with spin-polarized density functional theory (DFT) for chosen O_2–Ag(110) geometries. The DFT calculations are performed with the *Vienna Ab initio Simulation Package* (VASP) [29, 30] using an energy cut-off of 400 eV in the plane-wave basis set. We apply the projector augmented-wave method (PAW) [31, 32] to describe the electron–core interaction. The exchange-correlation energy is described by the Perdew-Burke-Ernzerhof (PBE) functional [33].

The calculated silver bulk lattice constant, $a = 4.16$ Å, compares well with the experimental value of 4.09 Å. The Ag(110) surface is modeled by a supercell consisting of a five-layer thick slab with 14 layers of vacuum and a (2×3) surface unit cell. As discussed below, the use of such a large supercell is necessary in the ulterior calculations of the O_2/Ag(110) DFT energies to avoid undesirable interactions among the periodically repeated molecules. The Brillouin-zone has been sampled with a $4 \times 4 \times 1$ Monkhorst-Pack grid of special **k**-points. Partial occupancies are determined by the Methfessel-Paxton method of order 1 with a smearing width of 0.2 eV. Keeping the middle layer frozen we allow relaxation of the other two layers from each side of the slab. As a result, the distance between the first and second layers reduces by -7.8%, and the distance between the second and third layers increases by $+3.6\%$. These results are in agreement with the experimental values of -7.8% and $+4.3\%$ [34]. Next, we calculate the binding energy, the bond length and the vibrational quanta of the O_2 molecule located in the middle of the vacuum region. At this position, there is no interaction between the molecule and the surface and the potential energy only depends on the O_2 interatomic distance r. Thus, after calculating the DFT energies for various r, we obtain from a simple spline interpolation the values of 5.88 eV for the bind-

ing energy (neglecting the zero point energy, ZPE) and 1.23 Å for the bond length. The vibrational quanta of 0.18 eV is calculated from the same potential energy $E(r)$ by solving numerically the radial Schrödinger equation. The results for the equilibrium bond length and vibrational quanta compare well with the corresponding experimental values of 1.21 Å and 0.19 eV [35]. Regarding the binding energy our value is somewhat higher than 5.12 eV, the experimental one [35]. This difference is consistent with the well known overestimation of the O_2 binding energy in vacuum at the DFT-GGA level. Nevertheless, since adsorption energies and dissociation barriers close to the surface are obtained from total energy differences involving configurations with relatively low density gradients, this overestimation is largely cancelled, and therefore, it is not expected to affect much the dissociation dynamics in the interpolated potential energy surface. Importantly, our results for O_2 midway the two Ag slabs confirm the adequacy of the supercell size used in our calculations. In addition, we further checked that upon increasing the surface unit cell to (3×4) all values remain practically the same. We note, that in all the calculations special care has been taken to obtain correct spin densities as we have verified that potential energies of the system are strongly dependent on the spin state.

After all these preliminary tests, we proceed to calculate the set of DFT energies that will be used to construct the 6D O_2/Ag(110) PES. In all the calculations, the relaxed geometry of the surface is kept frozen. For practical reasons, the reference zero potential energy is taken as that of the molecule in its equilibrium bond length ($r_0 = 1.23$ Å) placed at 6.0 Å from the surface. At this distance, the energy differs in less than 10 meV from the value obtained when the molecule is in the middle of the vacuum region and it justifies our choice. One convenient way of describing the six degrees of freedom of the molecule interacting with the frozen surface is by using the following coordinates depicted in Fig. 1(a): the cartesian coordinates that define the position of the center of mass of the molecule with respect to the surface (X,Y,Z), the O_2 interatomic distance r, and the polar and azimuthal angles (θ,φ) that define the orientation of the molecule. The DFT energy grid is constructed by computing two-dimensional (2D) (r,Z) cuts for different configurations of the O_2 molecule over the Ag(110) surface. Each configuration is defined by the center of mass coordinates (X,Y) and the O_2 orientation (θ,φ). In the 2D cuts r is varied from 0.93 Å to 2.53 Å in a non-equidistant grid of 13 points and Z is varied from 6.0 Å down to 0.0 Å in steps of 0.1 Å. The 2D cuts have been calculated for the five different (X,Y) positions shown by black circles

in Fig. 1(b). Four of them correspond to the most symmetrical sites on the surface. The fifth one corresponds to a non-symmetrical site that has been chosen in order to improve the quality of the CRP interpolation. For each site a different number of orientations have been considered. All in all, the 2D cuts have been calculated for the following 34 configurations:

- top site ($X = 0$, $Y = 0$) with seven orientations: $\theta = 0°$; $\theta = 45°$ with $\varphi = 0°,\ 35.26°,\ 90°$; $\theta = 90°$ with $\varphi = 0°,\ 35.26°,\ 90°$
- hollow site ($X = a/2$, $Y = a/(2\sqrt{2})$) with seven orientations $\theta = 0°$; $\theta = 45°$ with $\varphi = 0°,\ 35.26°,\ 90°$; $\theta = 90°$ with $\varphi = 0°,\ 35.26°,\ 90°$
- long-bridge site ($X = a/2$, $Y = 0$) with five orientations: $\theta = 0°$; $\theta = 45°$ with $\varphi = 0°,\ 90°$; $\theta = 90°$ with $\varphi = 0°,\ 90°$
- short-bridge site ($X = 0$, $Y = a/(2\sqrt{2})$) with five orientations: $\theta = 0°$; $\theta = 45°$ with $\varphi = 0°,\ 90°$; $\theta = 90°$ with $\varphi = 0°,\ 90°$
- top-hollow site ($X = a/4$, $Y = a/(4\sqrt{2})$) with ten orientations $\theta = 0°$; $\theta = 45°$ with $\varphi = 35.26°$, 90°, 144.74°, 215.26°, 270°, 324.74°; $\theta = 90°$ with $\varphi = 35.26°$, 90°, 144.74°.

To perform the 6D interpolation using the CRP [28] one also has to calculate the three dimensional (3D) PES of an atom interacting with the surface, in our case O with Ag(110). This 3D PES V^{3D} is then subtracted from the 6D PES V^{6D} to obtain the less corrugated function I^{6D} that can be accurately interpolated:

$$I^{6D}(X,Y,Z,r,\theta,\varphi) = V^{6D}(X,Y,Z,r,\theta,\varphi) \\ -V^{3D}(X_A,Y_A,Z_A) - V^{3D}(X_B,Y_B,Z_B)\,, \qquad (1)$$

where $(X_{A,B}, Y_{A,B}, Z_{A,B})$ are the cartesian coordinates of each atom of the molecule. After interpolating I^{6D}, the V^{3D} values are again added to the interpolation function to obtain the intended $V^{6D}(X,Y,Z,r,\theta,\varphi)$. A similar procedure is applied to obtain the requested $V^{3D}(X_{A,B}, Y_{A,B}, Z_{A,B})$ using in this case a one-dimensional (1D) O-Ag potential energy to reduce the corrugation of the 3D PES as prescribed in Ref. [28]. In our case, the atomic 3D O/Ag(110) PES is obtained from a grid of spin-polarized DFT energies that are calculated for the 25 sites illustrated by white and black circles in Fig. 1(b). For each site the distance of the atom to the surface is sampled from 6.0 Å to −1.2 Å in steps of 0.1 Å. After subtracting

the 1D O-Ag potential the resulting 3D interpolation function is interpolated by the 3D cubic spline method (more information in ESI). The method we use is the same as in Ref. [36]. The interpolation of I^{6D} is carried out in three steps. First, the (r,Z) interpolation is performed using the 2D cubic spline method. Subsequently, we interpolate over φ and θ using Fourier series expansions that take into account the symmetry of each particular site. Finally, the 2D cubic spline method is again applied for the (X,Y) interpolation (more information in ESI).

In order to benchmark the accuracy of our interpolation we perform various tests using DFT data not included in the construction of the interpolation function. Comparisons of the DFT and interpolated values are shown in Figs. 2, 3, and 4. The tests shown in Fig. 2 are done for the configurations for which one would expect the largest interpolation errors, that is, for (X, Y)-positions located halfway the sites used in the construction of the 6D PES and for (θ,φ) orientations not used in the DFT energy set. Extreme examples of the accuracy reached in the typically sensitive (θ,φ) interpolations are shown in Figs. 3 and 4. The selected configurations correspond to those showing the largest interpolation errors. In general, we observe that interpolation errors are small ($\sim$ 50 meV) in the majority of the molecule configurational space. For a small number of configurations, the accuracy is in the range of $\sim$ 100 meV when the molecule is close to the surface ($Z < 2$ Å), as can be seen in Fig. 4. However, errors in the important regions for the dynamics, such as adsorption sites and minimum energy barriers for reactions are kept below 20 meV. Errors are larger in highly repulsive regions ($>$ 5 eV), but these regions are not probed in the dynamics of the molecule.

III. PROPERTIES OF THE 6D POTENTIAL ENERGY SURFACE

A selection of 2D (r,Z) cuts of the O_2/Ag(110) PES is shown in Fig. 5. We choose these configurations because of their importance in either the dissociation or the O_2 adsorption processes. In the selected configurations the molecule center of mass is located at hollow, long-bridge, and short-bridge sites and with its axis oriented parallel to the surface ($\theta = 90°$) along the <001> ($\varphi = 0°$) and <1$\bar{1}$0> ($\varphi = 90°$) directions. Four of these configurations correspond to four distinctive adsorption wells, namely, hollow <1$\bar{1}$0> (denoted as H1$\bar{1}$0 in the following), hollow <001> (denoted H001), short-bridge <1$\bar{1}$0> (denoted SB1$\bar{1}$0) and

long-bridge <001> (denoted LB001). The same adsorption positions have been identified in Ref. [22] and, with the exception of SB1$\bar{1}$0, in Refs. [16–18]. Although the other two configurations in Fig. 5, short-bridge <001> (denoted SB001) and long-bridge <1$\bar{1}$0> (denoted LB1$\bar{1}$0), show also shallow minima in the 2D cuts, they do not correspond to adsorption wells because they are not minima in 6D. The values we obtain from the O_2/Ag(110) 6D PES for the adsorption energy E_a, the molecule-surface height Z, the interatomic distance r, and the spin-polarization per O_2 are shown in Table I for each adsorption well, together with values from Ref. [22] for comparison. Our values for Z and r agree well with those reported in Ref. [22], however, there are some differences in the depths of the wells that require some consideration.

In our frozen surface calculations, the deepest well is the SB1$\bar{1}$0 with an energy of −0.33 eV, very similar to the value of −0.27 eV reported by Roy *et al.* [22] for this site allowing surface relaxation. We have checked that the adsorption energy at this site does not change significantly when relaxing the surface. Since all important parameters of the calculation are similar in the two cases, we suspect that the difference of about 60 meV may be due to converging to different spin densities. In this respect, we have checked that at this site the energy is highly dependent on the magnetization of the system and that to converge to the spin density with the lowest energy one has to start with a good initial guess. The same considerations also hold for the LB001 adsorption site. In contrast, our adsorption energies for the H1$\bar{1}$0 and H001 wells are more than 100 meV smaller than in Ref. [22]. The differences are not related with the spin-polarization because it is practically zero, but to surface relaxation. In fact, we checked that when surface relaxation is allowed, the wells over hollow become the deepest and the (relaxed) energies are similar to those of Ref. [22]. Another remarkable feature of our 6D PES is the absence of energy barriers to access the adsorption wells, in accordance with previous DFT results [16–18, 22].

Our interpolated PES allows for a systematic exploration of the molecular configurational space to find the lowest energy barrier to dissociation [37]. Among all the configurations, the H1$\bar{1}$0 and the H001 are the ones that present the minimum energy barriers to dissociation with a value of 0.36 eV. In both cases, they are late barriers that appear at an interatomic distance of 2.0 Å. The existence of a minimum energy barrier that the molecules have to overcome in order to dissociate is in agreement with the lack of direct dissociation events at low incidence energies reported in molecular beam experiments [7, 10]. It is worth

to mention that even though the barriers for H1$\bar{1}$0 and H001 are of the same height and located at the same interatomic distance, the shape of these barriers and the neighboring energy landscape differ significantly from each other, as observed in Fig. 5. In the H1$\bar{1}$0 configuration, the potential energy decreases for $r > 2.0$ Å and it is already negative at our uttermost interatomic distance $r = 2.53$ Å. In contrast, for the H001 configuration, the potential energy remains almost constant for $r > 2.0$ Å. Previous DFT calculations give similar barrier heights [16–18, 22]. Figure 5 shows the existence of paths to dissociation also in the LB1$\bar{1}$0 and SB001 configurations but with higher energy barriers of ~ 0.7 eV and ~ 1.2 eV, respectively. Dissociation energy barriers for the selected configurations of Fig. 5 are shown in Table I. It is worth to mention that the minimum barrier to dissociation in Ag(110) (0.36 eV) is much lower than the minimum barriers to dissociation found in the two other low-index silver surfaces (1.05 eV for Ag(100) [25] and 1.1 eV for Ag(111) [26]). This is consistent with the experimentally observed more reactive character of the Ag(110) surface [4–10].

IV. DISSOCIATIVE STICKING OF O_2 MOLECULES ON THE Ag(110) SURFACE

The previous static analysis of the O_2/Ag(110) 6D PES that is focused on the 2D (r,Z) cuts, although informative, can be misleading because the actual reaction of the molecule with the frozen surface proceeds through a six-dimensional configurational space. Here we study the dissociative dynamics of O_2 on Ag(110) by performing classical and quasiclassical trajectory calculations in which the adiabatic force acting on the molecule is calculated with the 6D PES described in the previous section. For each incidence condition determined by the initial kinetic energy E_i and the incidence polar angle Θ_i, a conventional Monte Carlo procedure is used to sample all possible initial O_2 orientations (θ,φ) and lateral positions (X,Y). All trajectories start with the molecule at $Z = 6.0$ Å above the surface, where the potential energy is by definition zero for O_2 at its equilibrium bond length, $r_0 = 1.23$ Å. In the classical calculations, which neglect ZPE, the initial O_2 interatomic distance is precisely r_0. In the quasiclassical calculations, the ZPE or higher rovibrational energies are included in the initial conditions of the O_2 internal degrees of freedom by using the corresponding classical microcanonical distribution of r and its conjugate momentum p_r. In our case,

the ZPE and higher rovibrational energies are obtained by solving the radial Schrödinger equation for the potential energy $E(r)$ that is calculated with the molecule halfway between two slabs. We distinguish three possible outcomes of each trajectory: (i) reflection, if the molecule is scattered back and reaches the starting point $Z = 6.0$ Å with a positive velocity along the surface normal, (ii) dissociation, if the interatomic distance is larger than 2.5 Å (i.e. $r \gtrsim 2r_0$) with positive radial velocity, and (iii) molecular trapping, if after the maximum integration time of 15 ps, the molecule is neither reflected not dissociated. Trapping events are negligible for the incident energies studied here ($E_i > 0.1$ eV).

The initial dissociative sticking coefficient S_0, i.e., the adsorption probability at zero coverage, as a function of the incidence energy E_i is shown in Fig. 6(a). Dissociation probabilities are evaluated for each incidence condition (E_i, Θ_i) from the outcome of 50 000 trajectories. In all cases the $S_0(E_i)$ curves show the characteristic behavior of an activated system, which is typically associated to the existence of energy barriers to dissociation. Let us first concentrate on the results obtained from the classical calculations at normal incidence. There are no dissociation events or, more precisely, the dissociation probability is lower than 2×10^{-5} for incident energies below 0.9 eV. This energy threshold for dissociation is considerably larger than the barrier for dissociation of 0.36 eV found for the H1$\bar{1}$0 and H001 configurations. Such difference suggests that reaction takes place through a very reduced configurational space. Similar observations have been reported for N_2 dissociation on Fe(110) [38, 39]. Interestingly, the configurational space leading to O_2 dissociation on the Ag(100) [25] and also on the close-packaged Ag(111) [26] appears to be more accessible than the more reactive Ag(110).

A better understanding of the dynamics leading to dissociation can be obtained by looking at Fig. 7. This figure shows the (X,Y) position of the dissociating and reflecting molecules when they first arrive at $Z = 3, 2, 1.5$, and 0.8 Å along the incoming part of the trajectory. We observe that for the incidence conditions of 1.5 eV and 0° all the molecules can arrive at $Z = 3$ Å with no noticeably lateral displacement. The reason is that up to this distance the PES is similarly attractive for all molecular configurations and, therefore, the lateral corrugation is negligible. Interestingly, the dissociating molecules are already located within a 1 Å wide strip that spans through long-bridge and hollow sites. At $Z = 2$ Å, 9% of the molecules are reflected and there are less molecules near top sites. Dissociating molecules remain more or less in the same (X,Y) positions. Depopulation of the top site (now very

repulsive) becomes even more apparent when molecules reach $Z = 1.5$ Å. At this distance, almost half of the molecules are already reflected. Most of the molecules are already reflected before reaching $Z = 0.8$ Å. In fact more than 2/3 of the molecules that come that close to the surface will dissociate. At this distance, molecules are preferentially concentrated around the hollow site, but some of them still remain close to the long-bridge site.

Next we analyze in more detail the position and orientation of the molecules at the instant of dissociation, i.e., when its internuclear distance reaches 2.5 Å. Left panels of Fig. 8 show their corresponding φ-distribution and (X,Y) position for the incidence conditions, $E_i = 1.6$ eV and $\Theta_i = 0°$. The dissociated molecules are basically parallel to the surface with $\theta \approx 90° \pm 15°$ (not shown). It is apparent that molecules dissociate with their axis oriented close to the <1$\bar{1}$0> direction ($\varphi \approx 90°$). Additionally, a larger number of molecules dissociate close to the hollow site than close to the long-bridge site. This behavior can be well understood with the help of Figs. 9 (a) and (b). These figures show the distribution on (X, Y) of the minimum energy barriers to dissociation obtained in the (r, Z) configurational space when the molecule is oriented parallel to the surface ($\theta = 90°$) along the <1$\bar{1}$0> direction ($\varphi = 90°$) in Fig. 9(a) and along the <001> direction ($\varphi = 0°$) in Fig. 9(b) [40]. It is observed that the region with rather low barriers is much broader in the <1$\bar{1}$0> direction. This explains why molecules under normal incidence preferentially dissociate in this direction and not in the <001> direction although the minimum energy barrier heights are similar. Additionally, focusing on the <1$\bar{1}$0> direction, the fact that barriers are lower close to the hollow site explains why more molecules dissociate near the hollow site than close to the long-bridge site, where the energy barriers are around 0.3-0.4 eV larger. Figure 9(d) shows the distribution on (X, Y) of the minimum barriers to dissociation obtained in the (r, Z, θ, φ) configurational space. Interestingly, this distribution of barriers follows more closely than Fig. 9(a) the distribution of actual dissociation positions shown in the bottom-left panel of Fig. 8. This observation can be linked with the fact that dissociation also occurs for orientations different from $\varphi = 90°$ as shown in the φ-distribution of Fig. 8, though with lower probability.

The quasiclassical calculations performed at normal incidence show in Fig. 6(a) by comparison with the classical results that the dissociation probability $S_0(E_i)$ increases when the ZPE is included. In particular, the classical energy threshold for dissociation is reduced by more than 0.3 eV, even if the ZPE is 90 meV only. To explore in more detail the efficiency of

the vibrational energy, we have also calculated $S_0(E_i)$ when the molecule is initially excited in the first vibrational state ($n = 1$). Compared with the quasiclassical results for the ground vibrational state ($n = 0$), we first observe that there is a further reduction in the energy threshold to dissociation of around 0.3 eV despite the added vibrational quanta amounts to 0.18 eV. Noticeably, the vibrational energy is more efficient than the translational energy in promoting dissociation for the E_i-range studied here. In other words, the same 0.18 eV added into E_i produces less dissociation: $S_0(E_i, n = 1) > S_0(E_i + 0.18, n = 0)$. Still, the dissociation path is the same as in the classical calculations, i.e the initial (X, Y)-positions of the dissociating O_2 are located in a narrow strip that spans through long-bridge and hollow sites. The obtained increase in the dissociation probability can, thus, be attributed to the better conversion of the incidence energy to radial momenta when the molecule already starts with a non-zero vibrational energy. As originally argued by Polanyi and Wong [41] for the simpler gas-phase reactions case, the reason of large vibrational efficiency in late barrier systems can be naively understood in terms of the typical elbow plots associated with a dissociation configuration (for instance, see the 2D cut of H1$\bar{1}$0 in Fig. 5). The vibrational motion starts being perpendicular to the reaction coordinate while the molecule approaches the surface, but it ends up running parallel to the reaction coordinate when the molecule reaches the surface. Thus, in a late barrier system, the vibrationally excited molecule arrives at the barrier with part of its energy already conveniently localized in the degree of freedom where the barrier appears, what facilitates the system to overcome it. Similar findings regarding the efficiency of the vibrational energy in dissociation has been reported for other late barrier systems [42–45]. As here, the fact of finding a vibrational efficacy greater than one is simply showing that the average energy barriers encountered by the molecule are lower for the vibrationally excited than for the ground state molecule, as it was nicely demonstrated by Díaz and Olsen [44].

In the following we analyze with classical calculations the dependence of $S_0(E_i)$ on the polar incidence angle. Comparing the classical results shown in Fig. 6(a) for $\Theta_i = 0°$, 20°, and 35°, it is clear that $S_0(E_i)$ decreases as Θ_i increases. This decrease, however, does not follow a normal energy scaling, because we observe in Fig. 6(b) that for equal normal incidence energy ($E_i \cos^2 \Theta_i$), S_0 increases with Θ_i, i.e., with the total energy E_i. A similar behavior was observed for N_2 dissociation on Fe(110) and explained in terms of the low energy barriers existing in the entrance channel [38]. However, since there are no

entrance barriers to access the dissociating configurations in the O_2/Ag(110) PES, other factors should be causing the Θ_i-dependence in the present case as we discuss next.

When analyzing the dissociation dynamics under normal incidence in Fig. 7, we showed that in that case 6% of the molecules with initial energy of 1.5 eV arrive at $Z = 0.8$ Å before being reflected or dissociated. Additionally, 4.3% of the total number of molecules arrive at that distance and later dissociate. From a similar analysis for $\Theta_i = 35°$ and the same initial energy, we get that 3.5% of molecules arrive at $Z = 0.8$ Å, but that only 0.3% are dissociating molecules. This shows that the main difference between normal and off-normal incidence it is not the different number of molecules that arrive close to the surface, but the number of molecules that arriving close to the surface dissociate, 72% for 0° and only 9% for 35°. The comparison between the configurational space at the instant of dissociation shown in Fig. 8 serves to highlight important differences between the dissociation conditions at normal and off-normal ($\Theta_i = 35°$) incidence. We observe that dissociation at the hollow site is strongly reduced for $\Theta_i = 35°$. In addition, the φ-distribution changes drastically from the preferential $\varphi = 90°$ obtained at normal incidence to an axis orientation close to $\varphi \approx 60°$ (or symmetrically $\varphi \approx 120°$). To understand this finding, we show in Fig. 9(c) the distribution in (X, Y) of the minimum energy barriers to dissociation in the (r, Z) configurational space for the molecule oriented parallel to the surface along the $\varphi = 60°$ direction. The figure shows that for this molecular orientation the minimum energy barriers for dissociation, with values around 0.6-0.8 eV, are located in the X, Y positions where molecules, under $\Theta_i = 35°$ incidence angle, dissociate (see Fig. 8). The values of these energy barriers are clearly higher than 0.36 eV, which is the value found at the hollow site for the minimum energy barrier. Indeed, the fact that for off-normal incidence dissociation takes place through reaction paths with higher energy barriers explains the lower dissociation probabilities. However, it remains to be understood why dissociation occurs preferentially at these positions and with this orientation for off-normal incidence.

In order to understand this fact, we plot in Fig. 10 the (X, Y) contour plot of the potential energy calculated as an average on Z within the range $Z = 2{-}4$ Å for different φ-orientations. In all cases, the molecule lies parallel to the surface ($\theta = 90°$) with the gas-phase bond length $r_0 = 1.23$ Å. Off-normal incidence molecules, as they have initial parallel momenta, explore a large region of the X, Y configurational space at intermediate distances from the surface ($Z = 2 - 4$ Å). At these intermediate distances the O_2 interatomic distance is close to r_0.

Therefore, the average potential energy provides a meaningful measure of the attractive or repulsive character of the PES along the incoming part of the trajectory. More precisely, Figs. 10(a) and (b) show that molecules with small azimuthal angle φ are attracted to broad areas around the long-bridge site. In fact, we have verified that this behavior is fulfilled for angles $\varphi = 0° \pm 45°$. For larger φ, the incident O_2 starts to be attracted to the short-bridge site as shown in Figs. 10(c) and (d). Notice that the hollow site is not particularly attractive or repulsive at any φ. However, for the bridge sites there exist orientations ($\varphi = 0° \pm 45°$ for the long-bridge and $\varphi = 90° \pm 30°$ for the short-bridge) where the attractive parts of the PES are relatively broad in the (X, Y)-plane. Figures 9 and 10 together show that the most attractive regions for a given φ orientation present relatively high barriers for dissociation. The region near the long-bridge site with $\varphi \approx 60°$ (or symmetrically $\varphi \approx 120°$) represents a compromise between the attractiveness of the PES and the presence of not too high barriers to dissociation. This is the reason why this region is favored for dissociation under off-normal incidence. The figures also explain the lack of dissociation close to the short-bridge site. For the configurations for which the short-bridge region is attractive (Fig. 10(d)) the barriers to dissociation are very high (Fig. 9(a)).

It is worth to discuss our results in relation to the experimental findings. To this aim, we compare in Fig. 11 the experimental data of Ref. [10] with our classical results of the dissociative $S_0(E_i)$ obtained for normal incidence conditions. For completeness, we also show and compare the dissociative sticking coefficient obtained by similar adiabatic dynamics calculations on Ag(100) [25] and Ag(111) [26] to the experimental results of Ref. [6] and Ref. [46], respectively. We start noting that our results for dissociative adsorption show that the reactivity of O_2 on Ag(110) is much higher than the one obtained in the calculations for Ag(100) and Ag(111). This is apparent from the lower energy barrier obtained for dissociation, as explained above, but also from the actual values of the dissociation probabilities. For instance, at an initial energy of $E_i = 2.0$ eV and normal incidence we obtain a dissociation probability of $S_0 = 0.12$ in this surface, whereas in Ag(111) and Ag(100) the calculated dissociation probabilities for the same incidence conditions are $S_0 \approx 0.05$. These facts are consistent, at least qualitatively, with molecular beam experiments performed at a surface temperature of 300 K showing that the Ag(110) is the most reactive of the low-index (flat) Ag surfaces for O_2 dissociation [4, 6, 7, 10]. Nevertheless, we note that the dissociation measured in those experiments actually occurs for incidence energies below the barrier for

dissociation found here. In particular, the experimental initial sticking coefficient shows an activation energy of around 0.2 eV and takes values as high as $S_0 = 0.45$ for $E_i = 0.7$ eV and normal incidence. This discrepancy cannot be resolved by invoking non-adiabatic effects as was done to explain the dissociative adsorption of O_2 on aluminium surfaces [47, 48]. These effects generate energy barriers to dissociation in the entrance channel that would in general further reduce the calculated sticking probability as compared to our adiabatic results, worsening, instead of improving, the comparison with the experimental data.

All this leads us to suggest that the quantitative disagreement between the theoretical and the experimental S_0 curves is probably related to the existence of two different dissociation mechanisms. As discussed in Refs. [7, 9, 10], the dependence of the experimental S_0 on the surface temperature indicates that the dissociation measured at these low E_i cannot be attributed to the direct mechanism found here, but to dissociation events preceded by molecular chemisorption. Hence, the analysis of adsorption at this energy regime would require to go beyond the frozen surface approximation to incorporate energy exchange channels between the molecule and the surface. In this respect, let us just mention that it looks at this stage puzzling the fact that experimentally this process is reported to be activated (with the above mentioned 0.2 eV activation energy), whereas our results, in agreement with other DFT calculations [16–18], do not show any entrance barrier for molecular adsorption. A similar problem was found on the Ag(100) surface [6, 25].

V. SUMMARY

In summary, we have studied the interaction of the O_2 molecule and the Ag(110) surface with especial emphasis on the dissociation process, by means of a six-dimensional (6D) potential energy surface (PES) based on density functional theory (DFT) and the PBE exchange-correlation functional. The use of the *corrugation reducing procedure* to interpolate an extended set of spin-polarized DFT energies has allowed us to construct a high quality 6D PES for the O_2 molecule on the frozen Ag(110) surface. In agreement with previous DFT calculations [16–18, 22], we find that the O_2/Ag(110) system is characterized by the lack of energy barriers for molecular adsorption, the existence of four molecular adsorption wells with energies ranging between 0.2–0.3 eV, and the existence of a minimum barrier to dissociation of about 0.36 eV.

We have performed classical and quasiclassical molecular dynamics simulations on top of this DFT-PES for different incidence kinetic energies and polar angles of the molecular beam, calculated the corresponding initial sticking coefficient and obtained information on the dissociation paths. Our classical dynamical calculations show that under normal incidence conditions, no dissociation event is obtained out of 50 000 trajectories for initial translational energies below 0.9 eV. This value contrasts with the calculated minimum energy barrier to dissociation of 0.36 eV that is found for O_2 over the hollow site and oriented parallel to the surface along the $<1\bar{1}0>$ direction ($\varphi = 90°$). Such an energy mismatch is an indication of the very reduced configurational space leading to dissociation in this system. In fact, we observe that the dissociating molecules remain located along a narrow strip linking hollow and long-bridge sites even for an incidence energy as high as 1.6 eV. Furthermore, most of them still dissociate through configurations close to the minimum-energy-barrier configuration. Interestingly, for off-normal incidence ($\Theta_i = 35°$) the configuration that dominates dissociation is closer to the long-bridge site with the orientation ($\theta \approx 90°, \varphi \approx 60°$). The fact that close to the long-bridge site the barrier to dissociation is larger (0.7 eV) than in the hollow site implies a much lower dissociation probability and a higher threshold energy for dissociation at off-normal incidence.

The quasiclassical calculations performed for normal incidence reveal the high efficiency of the vibrational energy in promoting dissociation. By including the zero-point-energy of only 90 meV, the classical activation energy of 0.9 eV is reduced to about 0.6 eV. Moreover a further reduction of ca. 0.3 eV is obtained for O_2 initially excited in the first vibrational state. The efficiency of the vibrational against the translational energy is confirmed when comparing the quasiclassical dissociation probabilities obtained for the ground and the first vibrational states.

Finally, we want to emphasize that our results for O_2 dissociation on Ag(110) are consistent with the absence of direct dissociation at low incidence energies reported by different molecular beam experiments [7, 9, 10]. For higher incidence energies, the authors suggest that direct dissociation is actually masked by the more efficient indirect dissociation process that proceeds through the chemisorption state. The analysis of molecular adsorption and of the associated indirect channels to dissociation requires the incorporation of energy interchange between the molecule and the surface and it is beyond the scope of the present work. In this respect, further work along these lines will be possible by making use of the

six-dimensional DFT-PES introduced here.

ACKNOWLEDGMENTS

We acknowledge the Basque Departamento de Educación, Universidades e Investigación, the University of the Basque Country UPV/EHU (Grant No. IT-756-13) and the Spanish Ministerio de Economía y Competitividad (Grant No. FIS2013-48286-C2-2-P). Computational resources were provided by the DIPC computing center.

[1] K. Prince, G. Paolucci, and A. Bradshaw, Surf. Sci. **175**, 101 (1986).

[2] C. T. Campbell, Surf. Sci. **157**, 43 (1985).

[3] R. Guest, B. Hernnäs, P. Bennich, O. Björneholm, A. Nilsson, R. Palmer, and N. Mårtensson, Surf. Sci. **278**, 239 (1992).

[4] M. Spruit and A. Kleyn, Chem. Phys. Lett. **159**, 342 (1989).

[5] F. de Mongeot, U. Valbusa, and M. Rocca, Surf. Sci. **339**, 291 (1995).

[6] F. de Mongeot, M. Rocca, and U. Valbusa, Surf. Sci. **363**, 68 (1996).

[7] L. Vattuone, M. Rocca, C. Boragno, and U. Valbusa, J. Chem. Phys. **101**, 713 (1994).

[8] F. de Mongeot, M. Rocca, and U. Valbusa, Surf. Sci. **377-379**, 691 (1997).

[9] L. Vattuone, C. Boragno, M. Pupo, P. Restelli, M. Rocca, and U. Valbusa, Phys. Rev. Lett. **72**, 510 (1994).

[10] A. Raukema, D. A. Butler, and A. W. Kleyn, J. Phys.: Condens. Matter **8**, 2247 (1996).

[11] D. A. Outka, J. Stöhr, W. Jark, P. Stevens, J. Solomon, and R. J. Madix, Phys. Rev. B **35**, 4119 (1987).

[12] F. Bartolucci, R. Franchy, J. C. Barnard, and R. E. Palmer, Phys. Rev. Lett. **80**, 5224 (1998).

[13] T. Zambelli, J. V. Barth, and J. Wintterlin, J. Phys.: Condens. Matter **14**, 4241 (2002).

[14] J. R. Hahn and W. Ho, J. Chem. Phys. **123**, 214702 (2005).

[15] J. R. Hahn and W. Ho, J. Chem. Phys. **122**, 244704 (2005).

[16] P. Gravil, J. White, and D. Bird, Surf. Sci. **352-354**, 248 (1996).

[17] P. A. Gravil, D. M. Bird, and J. A. White, Phys. Rev. Lett. **77**, 3933 (1996).

[18] D. Bird and P. Gravil, Surf. Sci. **377-379**, 555 (1997).

[19] F. Olsson, N. Lorente, and M. Persson, Surf. Sci. **522**, L27 (2003).

[20] M. Alducin, D. Sánchez-Portal, A. Arnau, and N. Lorente, Phys. Rev. Lett. **104**, 136101 (2010).

[21] S. Monturet, M. Alducin, and N. Lorente, Phys. Rev. B **82**, 085447 (2010).

[22] S. Roy, V. Mujica, and M. A. Ratner, J. Chem. Phys. **139**, 074702 (2013).

[23] V. I. Pazzi and G. F. Tantardini, Surf. Sci. **377-379**, 572 (1997).

[24] V. I. Pazzi, P. H. T. Philipsen, E. J. Baerends, and G. F. Tantardini, Surf. Sci. **443**, 1 (1999).

[25] M. Alducin, H. F. Busnengo, and R. D. Muiño, J. Chem. Phys. **129**, 224702 (2008).

[26] I. Goikoetxea, J. Beltrán, J. Meyer, J. I. Juaristi, M. Alducin, and K. Reuter, New J. Phys. **14**, 013050 (2012).

[27] I. Goikoetxea, J. Meyer, J. I. Juaristi, M. Alducin, and K. Reuter, Phys. Rev. Lett. **112**, 156101 (2014).

[28] H. F. Busnengo, A. Salin, and W. Dong, J. Chem. Phys. **112**, 7641 (2000).

[29] G. Kresse and J. Furthmüller, Comput. Mater. Sci. **6**, 15 (1996).

[30] G. Kresse and J. Furthmüller, Phys. Rev. B **54**, 11169 (1996).

[31] P. E. Blöchl, Phys. Rev. B **50**, 17953 (1994).

[32] G. Kresse and D. Joubert, Phys. Rev. B **59**, 1758 (1999).

[33] J. P. Perdew, K. Burke, and M. Ernzerhof, Phys. Rev. Lett. **77**, 3865 (1996).

[34] Y. Kuk and L. C. Feldman, Phys. Rev. B **30**, 5811 (1984).

[35] D. R. Lide, ed., *CRC Handbook of Chemistry and Physics*, 86th ed. (2005).

[36] M. Alducin, R. Díez Muiño, H. F. Busnengo, and A. Salin, J. Chem. Phys. **125**, 144705 (2006).

[37] We use a simple (brute force) method that consists in exploring the entire configurational space by making loops over a fine grid mesh of the six variables of the O_2/Ag(110) PES. More precisely, for each configuration defined by the set of coordinates $(X, Y, Z, \theta, \varphi)$ we find the maximum energy value when increasing r. In this way, we obtain the dissociation energy value for each configuration. By selecting the minimum of these energy values we obtain the minimum dissociation barrier and the corresponding coordinates define the transition state configuration.

[38] I. Goikoetxea, M. Alducin, R. Díez Muiño, and J. I. Juaristi, Phys. Chem. Chem. Phys. **14**, 7471 (2012).

[39] I. Goikoetxea, J. I. Juaristi, R. Díez Muiño, and M. Alducin, Phys. Rev. Lett. **113**, 066103 (2014).

[40] The procedure is similar to [37] but for fixed (θ, φ).

[41] J. C. Polanyi and W. H. Wong, J. Chem. Phys. **51**, 1439 (1969).

[42] M. J. Murphy, J. F. Skelly, A. Hodgson, and B. Hammer, J. Chem. Phys. **110**, 6954 (1999).

[43] R. R. Smith, D. R. Killelea, D. F. DelSesto, and A. L. Utz, Science **304**, 992 (2004).

[44] C. Díaz and R. A. Olsen, J. Chem. Phys. **130**, 094706 (2009).

[45] B. Jiang, X. Ren, D. Xie, and H. Guo, PNAS **109**, 10224 (2012).

[46] A. Raukema, D. A. Butler, F. M. Box, and A. W. Kleyn, Surface Science **347**, 151 (1996).

[47] G. Katz, Y. Zeiri, and R. Kosloff, Isr. J. Chem. **45**, 27 (2005).

[48] J. Behler, B. Delley, S. Lorenz, K. Reuter, and M. Scheffler, Phys. Rev. Lett. **94**, 036104 (2005).

TABLE I. Properties of the adsorption states O_2 on Ag(110): Adsorption energy E_a, O_2-surface distance Z, interatomic O-O distance r, spin polarization of the system (sp) in units of the Bohr magneton, and energy barriers to dissociation E_d. Values from Ref. [22], which include surface relaxation, are listed within brackets.

Site	E_a (eV)	Z (Å)	r (Å)	sp (μ_B)	E_d (eV)
H1$\bar{1}$0	0.21(0.37)	1.09(1.01)	1.45(1.45)	0.08	0.36
H001	0.24(0.37)	1.29(1.22)	1.42(1.42)	0.00	0.36
SB1$\bar{1}$0	0.33(0.27)	2.20(2.15)	1.31(1.31)	1.27	>2
SB001	-	-	-	-	1.2
LB001	0.24(0.23)	1.98(1.92)	1.29(1.31)	1.30	>2
LB1$\bar{1}$0	-	-	-	-	0.7

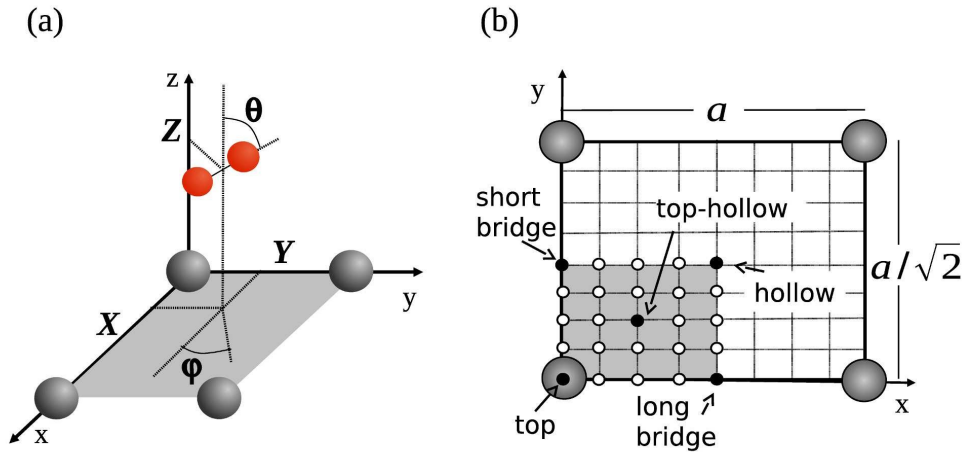

FIG. 1. (a) Coordinate system used in our calculations: Ag atoms are in grey and the O atoms are in red. The x- and y-axis are parallel to the <001> and <1$\bar{1}$0> directions, respectively. (b) Geometry of the Ag(110) surface. DFT calculations of the O/Ag(110) PES have been performed for all sites marked by white and black circles. For O_2/Ag(110), DFT calculations have been performed for configurations with the molecular center of mass over the sites marked by black circles. The shaded area shows the irreducible surface unit cell.

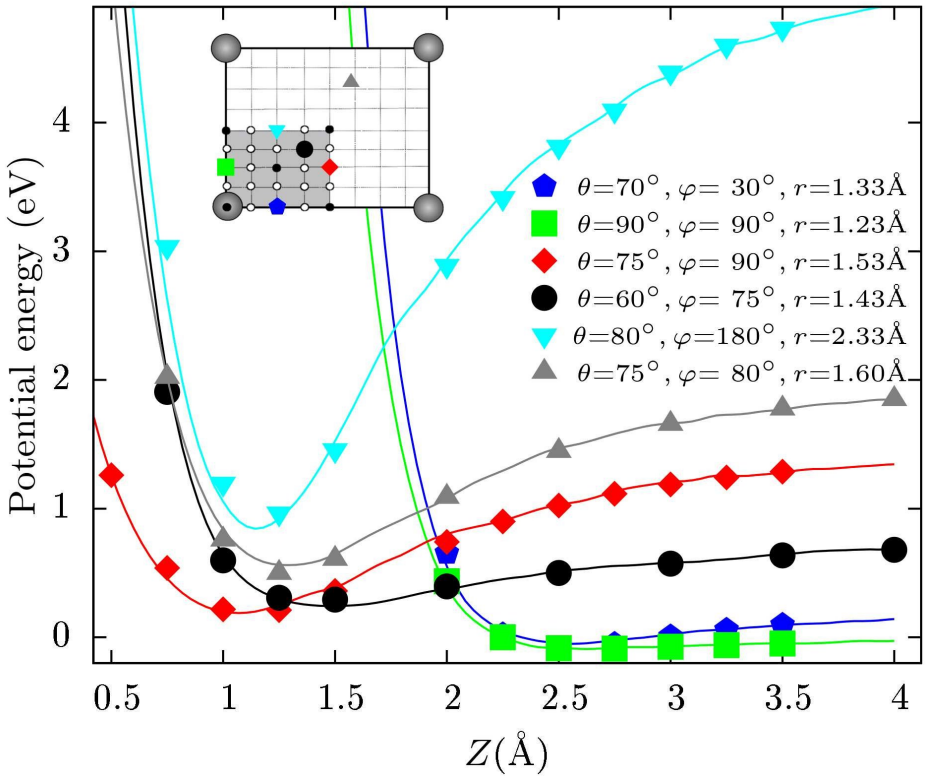

FIG. 2. Potential energy as a function of the O_2 center of mass height Z. The interpolated potential energies (lines) are compared with their corresponding DFT values (symbols) for different O_2 configurations $(X, Y, r, \theta, \varphi)$ not used in the interpolation procedure. The (X, Y) positions are marked on the Ag(110) cell by the corresponding DFT symbols.

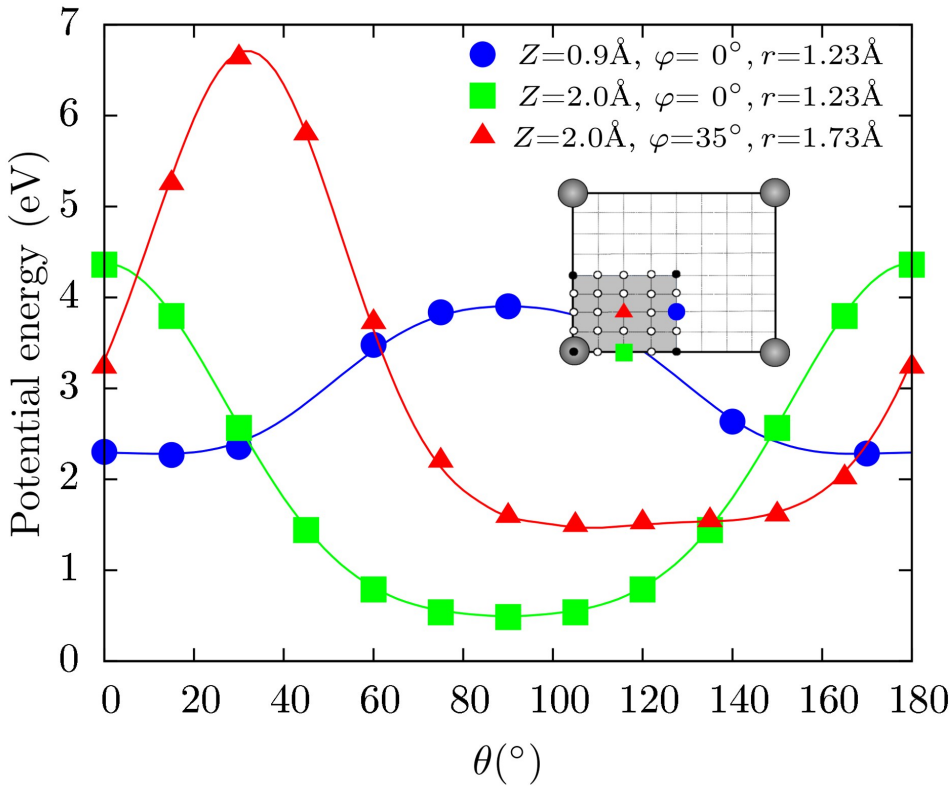

FIG. 3. Potential energy as a function of the O_2 polar angle θ. The interpolated potential energies (lines) are compared with their corresponding DFT values (symbols) for different O_2 configurations (X, Y, Z, r, φ) not used in the interpolation procedure. The (X, Y) positions are marked on the Ag(110) cell by the corresponding DFT symbols.

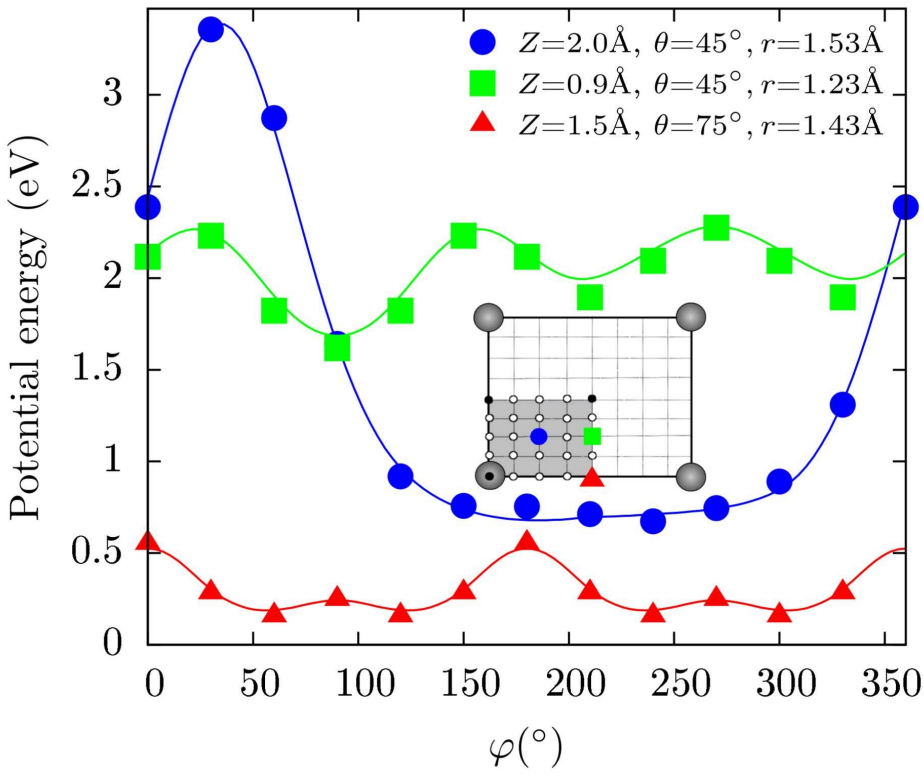

FIG. 4. Potential energy as a function of the O_2 azimuthal angle φ. The interpolated potential energies (lines) are compared with their corresponding DFT values (symbols) for different O_2 configurations (X, Y, Z, r, θ) not used in the interpolation procedure. The (X, Y) positions are marked on the Ag(110) cell by the corresponding DFT symbols.

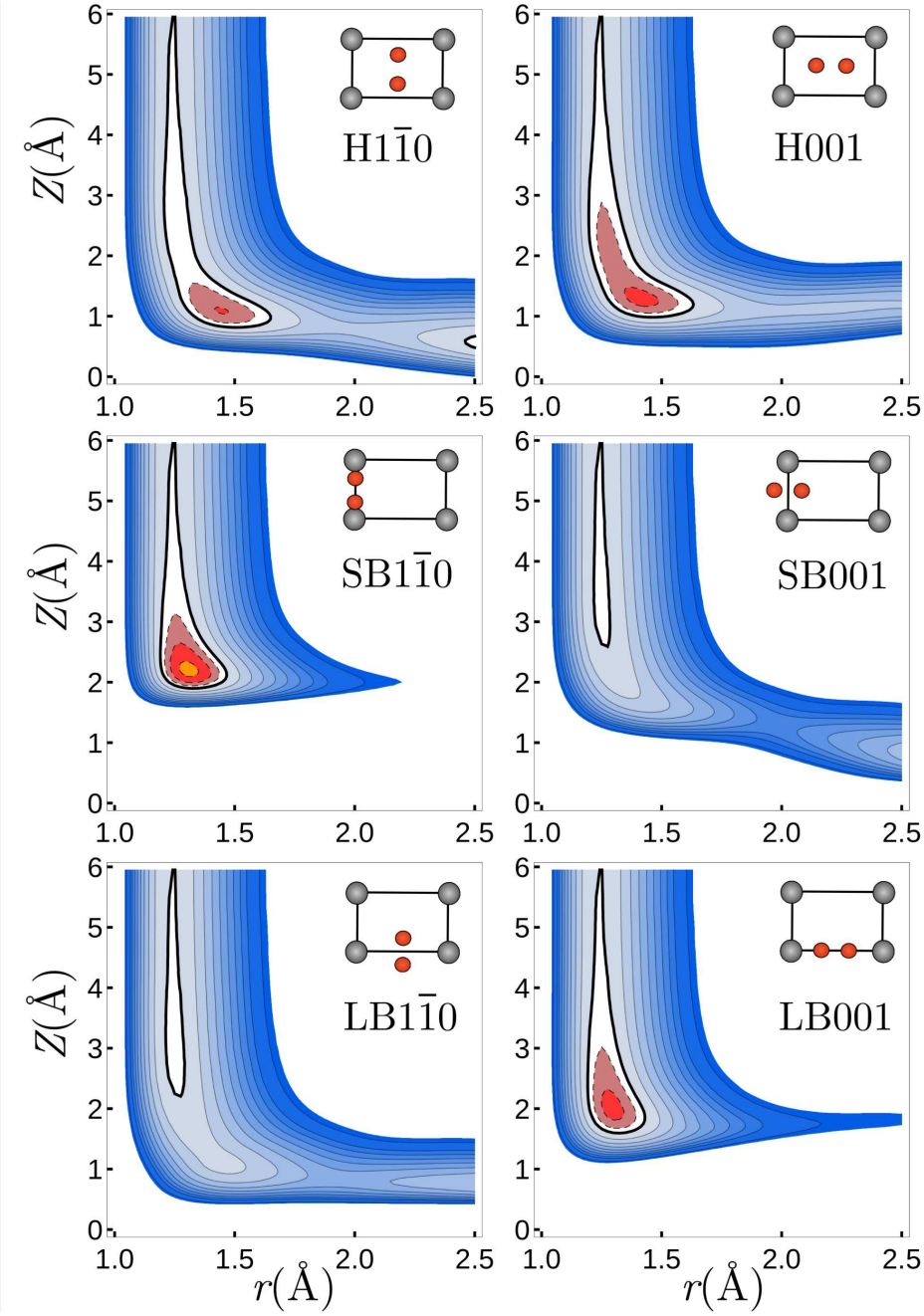

FIG. 5. (r, Z)-cuts of the O_2/Ag(110) 6D PES. The molecular orientation and position over the surface unit cell is schematically depicted in each contour plot. All molecules are positioned parallel to the surface ($\theta = 90°$). Solid (dashed) contour lines correspond to positive (negative) values of the potential energy and separate intervals of 0.2 eV (0.1 eV). Thick solid lines correspond to zero potential energy.

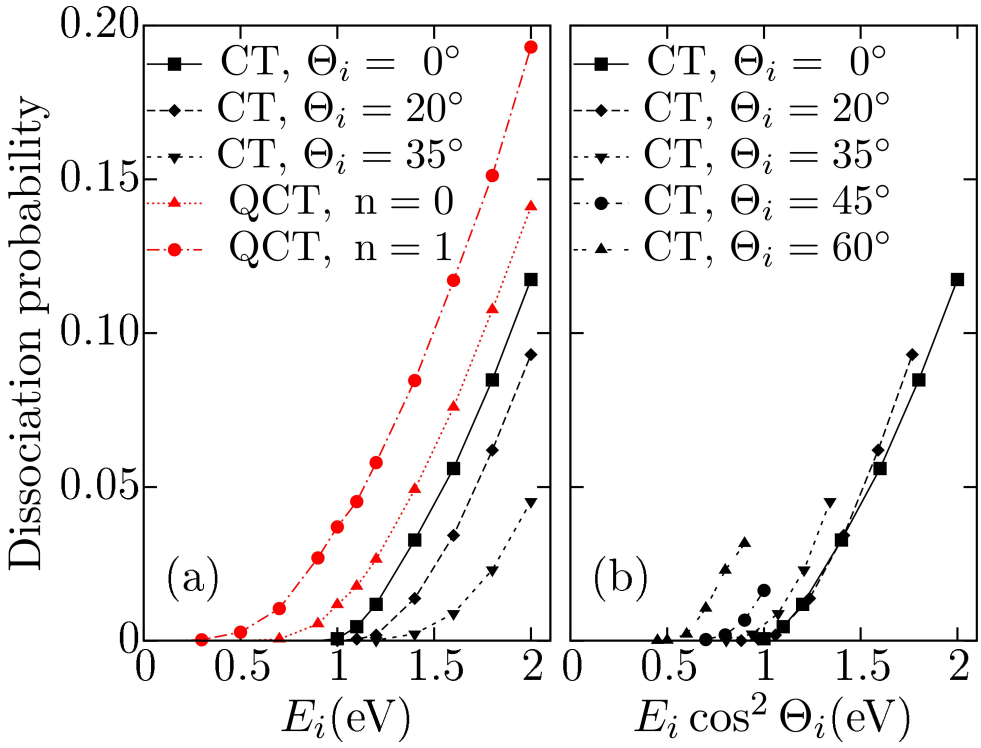

FIG. 6. Initial dissociative sticking coefficient S_0 as a function of (a) the initial kinetic energy E_i and (b) the initial normal energy $E_i \cos^2 \Theta_i$. Black curves: classical trajectory (CT) calculations performed for different incidence angles Θ_i. Red curves: quasiclassical trajectory (QCT) calculations performed at normal incidence ($\Theta_i = 0$) for the ground (n=0, ZPE) and the first excited (n=1) vibrational states.

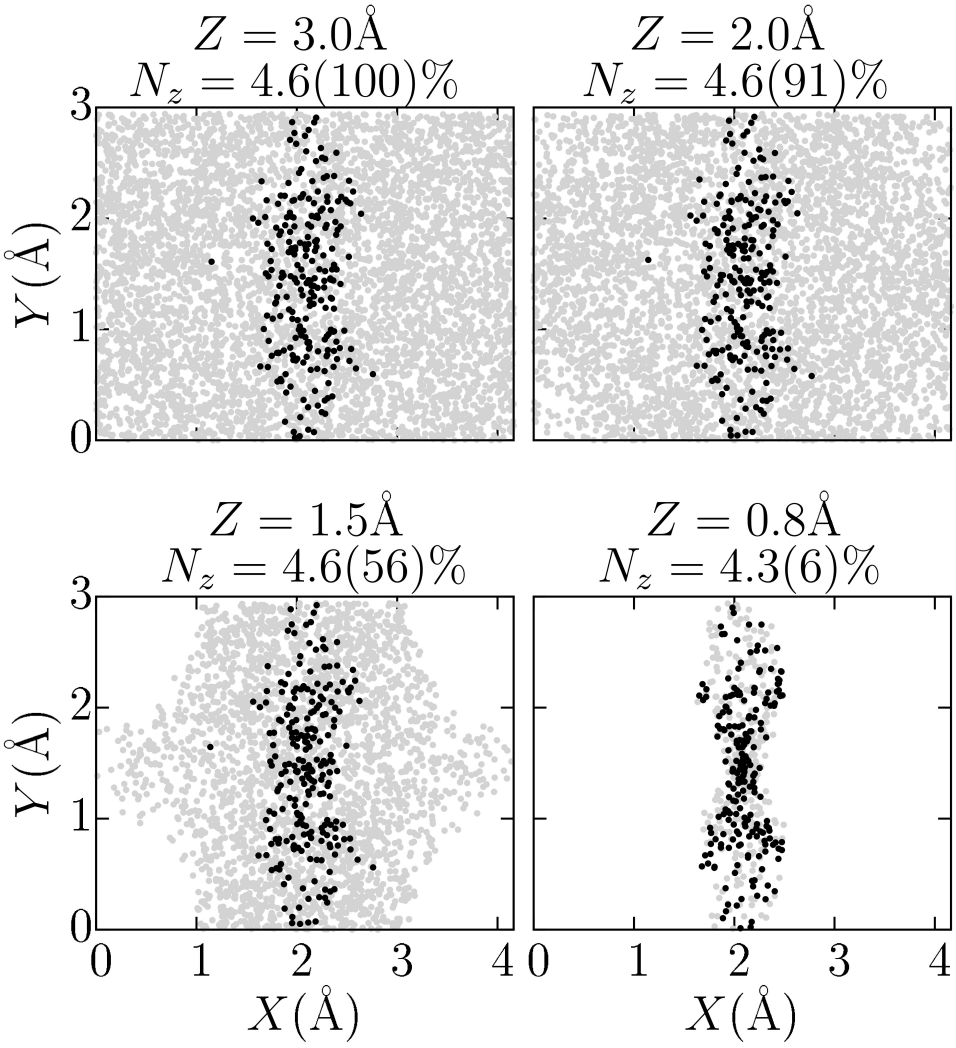

FIG. 7. Position of the O_2 center of mass over the surface unit cell when first reaching the height Z written above each panel. The dissociating and reflecting molecules are plotted by black and grey circles, respectively. On top of each panel, N_z denotes the fraction of dissociating molecules reaching Z, while the total percentage of molecules at each Z is written within the parenthesis. Data obtained from 5 000 trajectories for E_i= 1.5 eV and $\Theta_i = 0°$. The sticking coefficient is 4.6%.

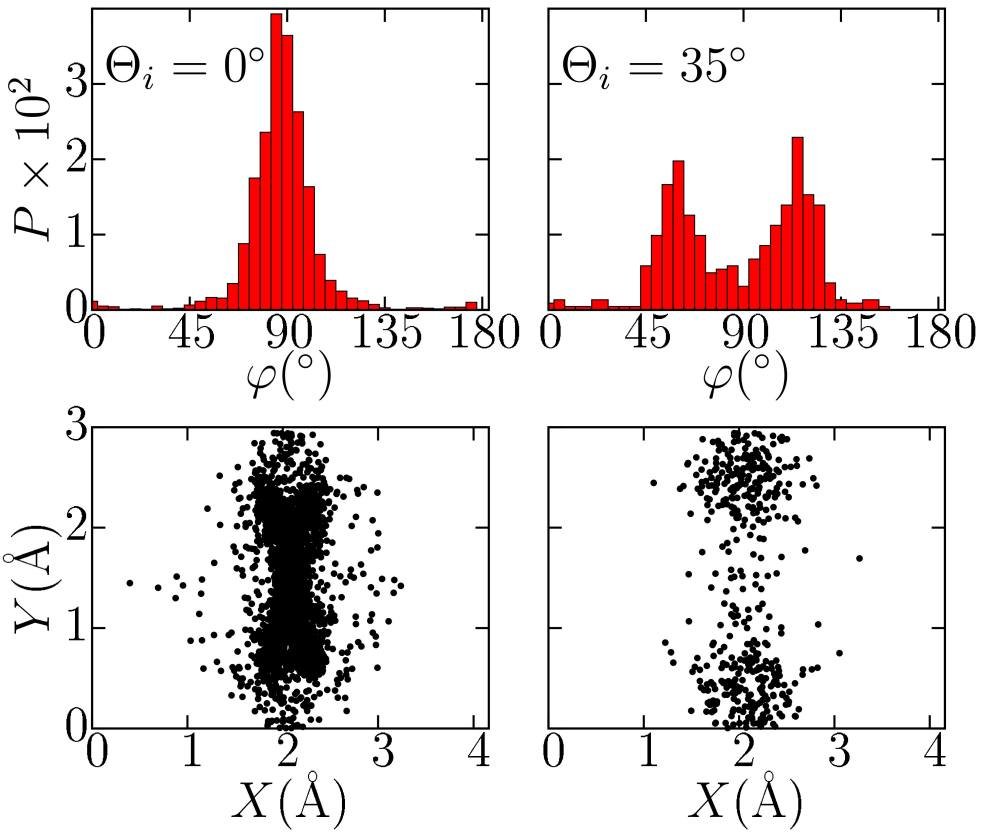

FIG. 8. Distribution of the azimuthal angle φ (top panels) and (X, Y)-positions of the O_2 center of mass (bottom panels) at the moment when the interatomic distance is maximal $r = 2.5$ Å. The φ-distributions are multiplied by 100. Results obtained from 50 000 trajectories for $E_i = 1.6$ eV and incidence angles $\Theta_i = 0°$ (left panels) and $\Theta_i = 35°$ (right panels).

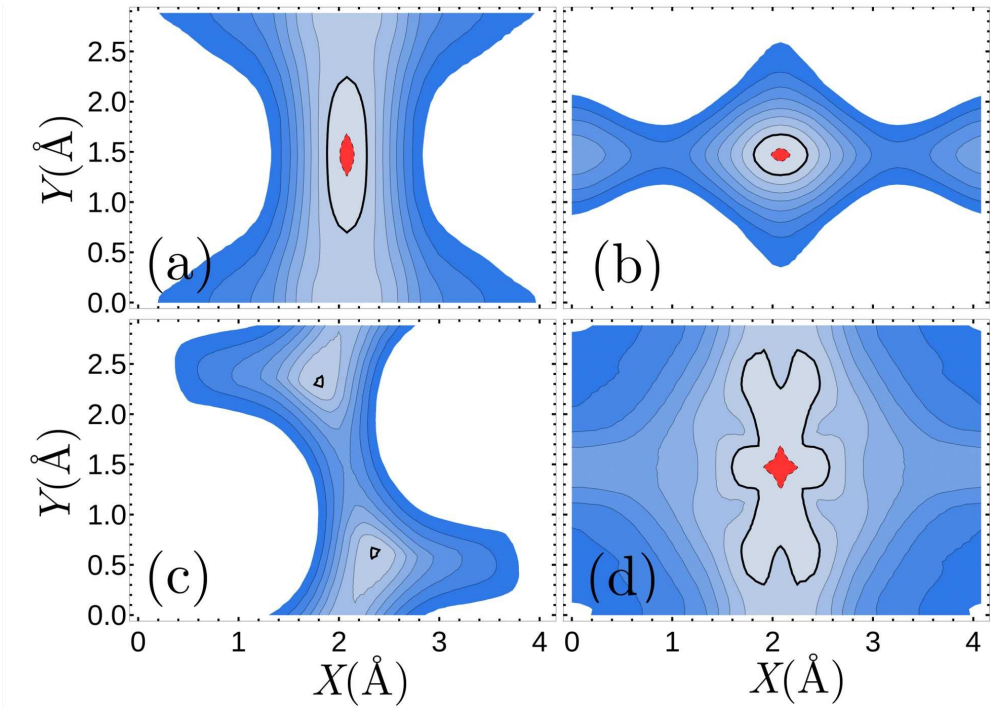

FIG. 9. Dependence of the minimum energy barriers to dissociation on the X, Y position of the center of mass of the molecule. In panels (a), (b) and (c) the minimum barrier is calculated in the two dimensional (r, Z) configurational space for the following molecular orientations: (a) $\theta = 90°$ and $\varphi = 90°$, (b) $\theta = 90°$ and $\varphi = 0°$, (c) $\theta = 90°$ and $\varphi = 60°$. In panel (d) the minimum barrier to dissociation is calculated in the four dimensional (r, Z, θ, φ) configurational space. Every contour line separates intervals of 0.2 eV. In the red area barriers are lower than 0.4 eV. The thick contour line corresponds to a value of 0.6 eV.

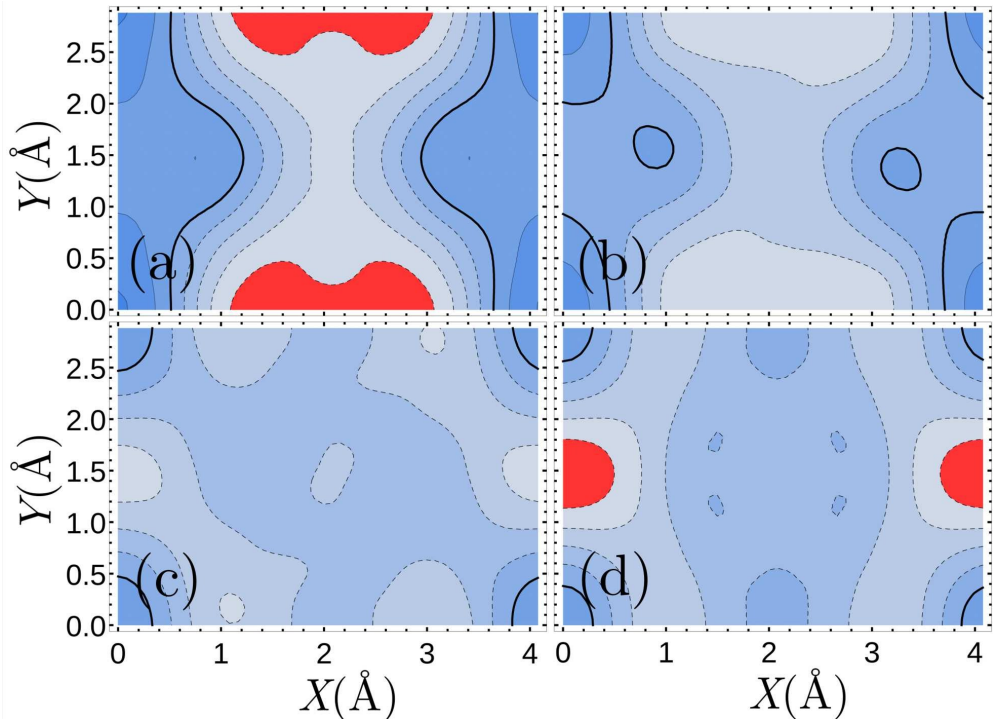

FIG. 10. Average on Z of the potential energies of the molecule as a function of the X, Y position of its center of mass for the equilibrium interatomic distance $r_0 = 1.23$ Å. The Z-range considered goes from $Z = 2$ Å up to $Z = 4$ Å. The molecule is oriented parallel to the surface ($\theta = 90°$) with: (a) $\varphi = 0°$, (b) $\varphi = 30°$, (c) $\varphi = 60°$, (d) $\varphi = 90°$. Every contour line separates intervals of 0.025 eV. In the red area the average potential energy is lower than -0.1 eV. The thick contour line corresponds to an average potential energy of 0.0 eV.

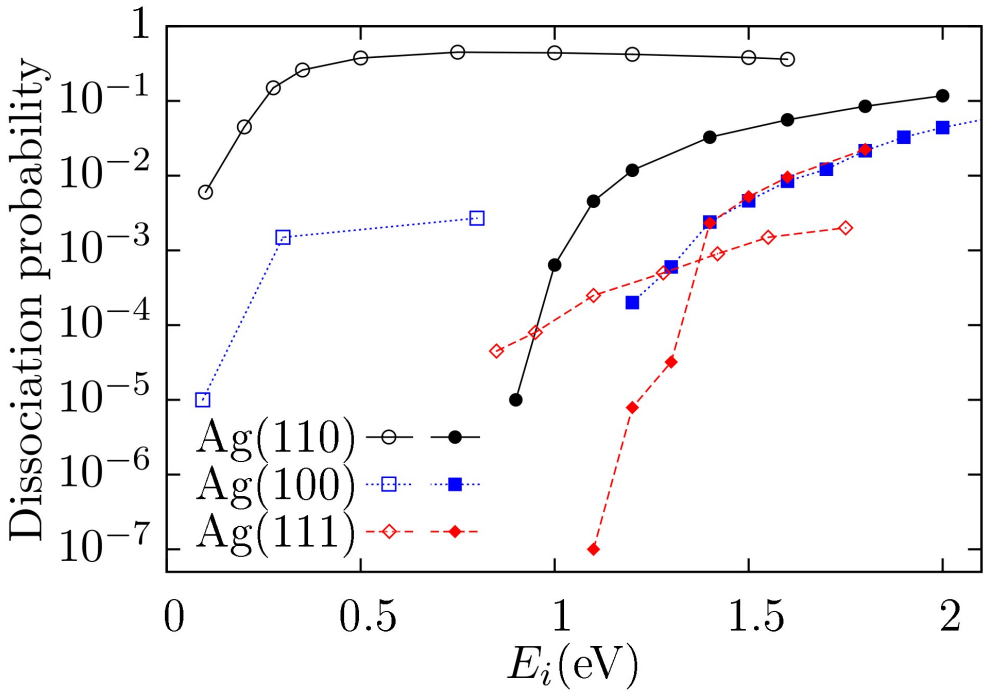

FIG. 11. Initial dissociative sticking coefficient S_0 as a function of the initial kinetic energy E_i at normal incidence ($\Theta_i = 0$). Comparison of experimental molecular beam results performed at surface temperatures $T_s \geq 300$ K (open symbols) and classical trajectory calculations (full symbols) for flat Ag surfaces. Black lines represent Ag(110) ([10], this work), blue lines represent Ag(100) ([6],[25]) and red lines represent Ag(111) ([46], [26]).